



HAL
open science

Erosion threshold of a liquid immersed granular bed by an impinging plane liquid jet

Sarah Badr, Georges Gauthier, Philippe Gondret

► **To cite this version:**

Sarah Badr, Georges Gauthier, Philippe Gondret. Erosion threshold of a liquid immersed granular bed by an impinging plane liquid jet. *Physics of Fluids*, 2014, 26 (2), pp.023302. 10.1063/1.4863989 . hal-04009882

HAL Id: hal-04009882

<https://hal.science/hal-04009882>

Submitted on 10 Mar 2024

HAL is a multi-disciplinary open access archive for the deposit and dissemination of scientific research documents, whether they are published or not. The documents may come from teaching and research institutions in France or abroad, or from public or private research centers.

L'archive ouverte pluridisciplinaire **HAL**, est destinée au dépôt et à la diffusion de documents scientifiques de niveau recherche, publiés ou non, émanant des établissements d'enseignement et de recherche français ou étrangers, des laboratoires publics ou privés.

Erosion threshold of a liquid immersed granular bed by an impinging plane liquid jet

Sarah Badr, Georges Gauthier and Philippe Gondret^{1, a)}

FAST, Université Paris Sud and CNRS (UMR 7608), Bât. 502 Campus

Universitaire F-91405 Orsay cedex, France

(Dated: 8 November 2013)

Erosion threshold of a model granular bed by a liquid jet in a quasi bidimensional configuration has been studied experimentally in both laminar and turbulent regimes. The jet is a thin sheet which impinges normally a packing of immersed beads monodisperse in size and density. The erosion threshold has been characterized at different impact distances of the jet on the sediment and for different grain size and fluid viscosity. In the explored range of parameters, we show that the erosion threshold is well described by a critical inertial Shields number based on the local flow velocity at the impinging point. This has been done by a careful analysis of the different jet flow regimes taking into account the position of the virtual origin of the jet.

^{a)}Electronic mail: name@fast.u-psud.fr

I. INTRODUCTION

Erosion processes are one of the key processes exhibited by granular material encountered in numerous and varied situations both natural and industrial.¹ For instance, erosion is a key phenomenon for the understanding of the geomorphological patterns on Earth or other planets or for the evolution of estuaries and river beds.² In Nuclear Engineering erosion is used for the dispersion of particulate fission products in High Active Storage Tank,³ and in aerospace industry soil erosion may involve damaging problems for rotorcraft vehicles⁴ or soil instability during rocket landings.⁵ But, since erosion is at the origin of the majority of dam and embankment failures,⁶ it is its civil engineering and societal stake that explain the large amount of studies devoted to this problem. Thus, the characterization of soil stability by reliable tests is the basis of diagnosis and understanding of risks that may come from the design of civil engineering structures. Over the last 50 years several apparatus have been designed to measure soil stability or embankment resistance.⁷ Among them one of the most used is the “Jet Erosion Test”,⁸ that consists in measuring the eroded mass and depth from the crater generated by the action of a water jet impacting the soil. Such a configuration present some strong facilities from a practical point of view, *e.g.* a simple use in the field, but also some difficulties of interpretation,^{9,10} even for a cohesionless soil where erosion is considered as a simple particle problem. These difficulties to interpret the results of the Jet Erosion Test mainly arise from the strong non uniform flow with a stagnation point at the bottom of the jet axis. As jet flows on solid walls has strong applications for cooling purposes,¹¹ the jet flow has been yet widely studied both experimentally and theoretically in both circular (3D)^{12–15} or plane (2D)^{14,16–18} cases, with some possible strong influence of finite aspect ratio¹⁹ or sidewalls,^{20–22} top endwall²² in the plane configuration, and also of porous endwall.^{23,24} With the jet flow characterization, different models have been proposed for describing the time evolution of the eroded crater by an impinging jet and its asymptotic shapes at rest after the jet stops or when it comes from a dynamical equilibrium of the erosive fluid forces with the restoring gravity forces.^{5,8,25–28} In all these studies, the erosion threshold is supposed to be the key parameter, together with the detailed knowledge of the downstream evolution of the jet, to explain the crater evolution above threshold. But the soil cratering induced by the erosion process affects back the flow field⁵ and thus the erosive strength of the jet. To avoid this feedback that complicates the interpretation, we focus

in the present paper on the erosion threshold by measuring the first grain displacements before the flat soil surface is modified, in the spirit of what has already been performed in homogeneous parallel shear flow within laminar^{29,30} or turbulent^{31–33} conditions. Such a detailed study of the erosion threshold of an horizontal granular bed from a jet flow has not still been made and may allow a better understanding of the subsequent cratering above threshold that may inferred from dimensional analysis either in plane (2D)³⁴ or axisymmetric (3D)³⁵ cases with turbulence analysis. We restrict the study to stationary jet flux which is clearly different from the pulsating flow where vortex shedding is enhanced and govern the erosion processes.³⁶

This paper reports experimental results of the erosion threshold due to an impinging plane jet on a flat cohesionless sediment in both laminar and turbulent regimes. A detailed analysis of the erosion threshold dependence with the distance between the jet nozzle and the bed surface is presented in terms of an inertial local Shields number that takes into account the spatial evolution of the jet downstream its virtual origin.

II. SET-UP

The experimental setup is composed of a horizontal bed of glass beads, of density $\rho_s = 2.5 \times 10^3 \text{ kg/m}^3$ and diameter d , immersed in a fluid of density ρ and dynamic viscosity η . A vertical sheet of the same fluid issuing from a plane injector of internal thickness $b = 4 \text{ mm}$ at a distance l from the bed surface impacts it normally. The bed is contained in a rectangular tank of height $H = 50 \text{ cm}$, width $L = 20 \text{ cm}$ and thickness $W = 3 \text{ cm}$. The sieved glass beads have a relative dispersion of 10% in size around their mean diameter d and the explored range of grain size ($0.1 < d < 1 \text{ mm}$) is such as the grain size is small compared to the jet thickness ($d/b < 1$). The fluid used is water most of the time, but aqueous solutions of glycerol are also used to vary the fluid kinematic viscosity $\nu = \eta/\rho$ in the range $10^{-6} \lesssim \nu \lesssim 4 \times 10^{-6} \text{ m}^2/\text{s}$ without varying significantly its density $\rho \simeq 10^3 \text{ kg/m}^3$. The injector is a tube of length 20 cm with a rectangular cross section of thickness $b = 4 \text{ mm}$ and width $w_J = 2.4 \text{ cm}$ slightly smaller than the tank thickness W , leading to a plane jet of aspect ratio $w_J/b = 6$. The volume flow rate Q is varied using a pump allowing fluid circulation without significant noise. From the calibration of the pump in the using conditions, the mean flow velocity of the jet at the injector outlet $U_J = Q/(b w_J)$ is controlled in the range

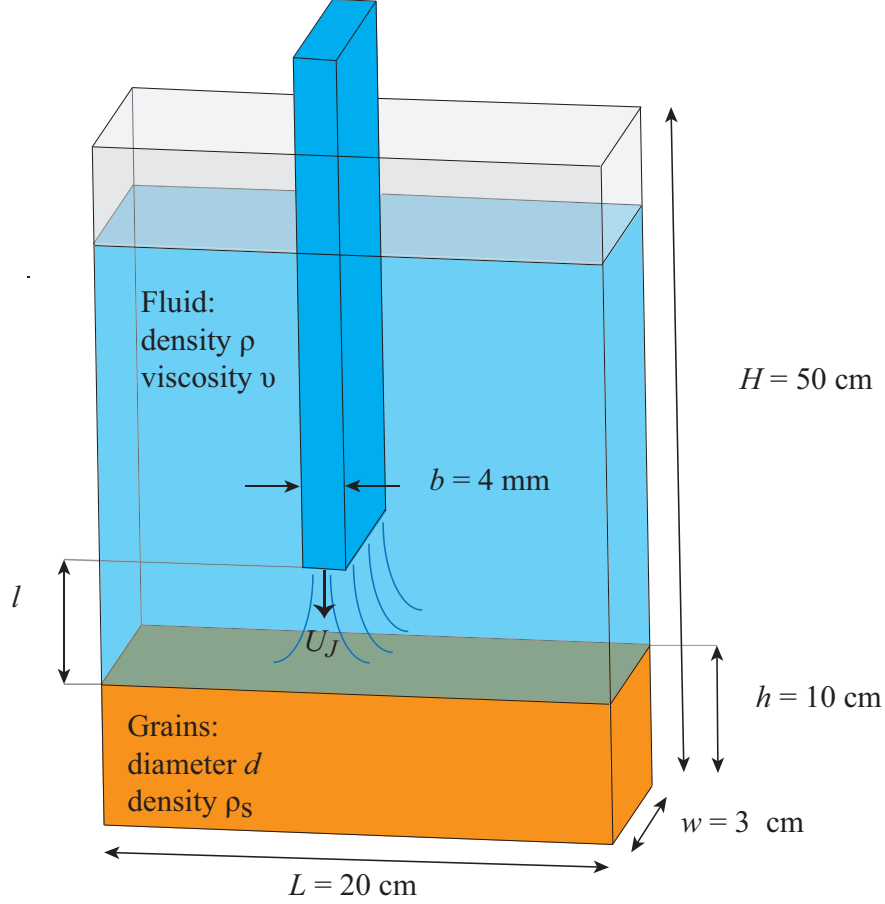


FIG. 1. Sketch of the experimental set-up.

$0 \lesssim U_J \lesssim 1 \text{ m/s}$.

Considering the numerous parameters of the experiments, many non dimensional parameters can be considered, but we will focus on the three following relevant controlled parameters:

$$Re_J = \frac{U_J b}{\nu}, \quad Sh_J = \frac{\rho U_J^2}{(\rho_s - \rho) g d}, \quad l^* = \frac{l}{b},$$

where Re_J is the Reynolds number that characterizes the ratio between inertial and viscous fluid forces in the jet flow, Sh_J is the Shields number corresponding to the ratio between the typical fluid force of the jet on a grain and its apparent weight, and l^* is the distance between the injector and the granular bed normalized by the jet thickness b . Note that this Shields number, which is sometimes referred as a densimetric Froude number,^{25,26} is here based on the fluid inertial stress and not on the viscous stress, which will be justified in the following as the particle Reynolds number remains larger than one. We have checked that other non dimensional parameters such as the aspect ratios L/b or h/d based on the length

L of the cell and the height h of the bed do not play any significant role in the problem as they are kept large enough ($L/b, h/d \gg 1$). In the following, we will present the results of erosion threshold as a function of the three non dimensional parameters presented above: The jet Reynolds number Re_J , the inertial Shields number Sh_J and the non dimensional jet-bed distance l^* . The experiments have been carried out in the following way. First, the grains are fluidized thanks to a vertical upward fluid injection through the porous bottom of the cell. Fluidisation is then stopped to let the grains settle and form a horizontal bed of reproducible solid volume fraction $\phi \simeq 0.6$. After the injector is set at a defined distance l from the bed surface, the jet velocity U_J is gradually increased up to first grains are seen to be displaced. This procedure is repeated about ten times to quantify the dispersion of the measurements around mean values.

III. EXPERIMENTAL RESULTS

Measurements of the jet velocity U_J at the erosion threshold of the granular bed are shown in Fig. 2a in terms of the jet Reynolds number Re_J as a function of the non dimensional distance l^* from the jet nozzle to the granular bed for three fluid/grain configurations with two grain diameters ($d = 0.25$ and 1 mm) and two fluid viscosities ($\nu = 10^6$ and 4×10^{-6} m²/s). As expected, the critical jet velocity and thus the corresponding Re_J for erosion increases with l^* , but data of Fig. 2a show non trivial complex curve shapes that let expect the existence of different regimes. The jet behavior is indeed different depending on the jet Reynolds number and nozzle-sediment distance l^* . For a free jet far from any boundaries ($l^* \gg 1, w_J/b \gg 1$), the transition from laminar regime to turbulent regime is known to happen for a critical Reynolds number Re_J of a few hundreds ($10^2 < Re_J < 10^3$).¹³ Our own jet visualizations with dye injection indeed reveal that the jet remains laminar (see Fig. 2b) for roughly $Re_J \lesssim 200$, and the corresponding horizontal dashed line $Re_J = 200$ is drawn in the (Re_J, l^*) diagram of Fig. 2a, even if this critical value may decrease slightly with increasing l^* . For large enough Re_J and l^* , the jet appears to be turbulent (Fig. 2d) with a strong expansion downstream of a small straight smooth zone usually referred as the potential core. When the jet is close enough to the bed surface ($l^* \lesssim 8$), there is not enough distance for the shear layers to develop and the jet core remains potential whatever the Reynolds number. For intermediate distances ($8 \lesssim l^* \lesssim 35$), the jet is known to show

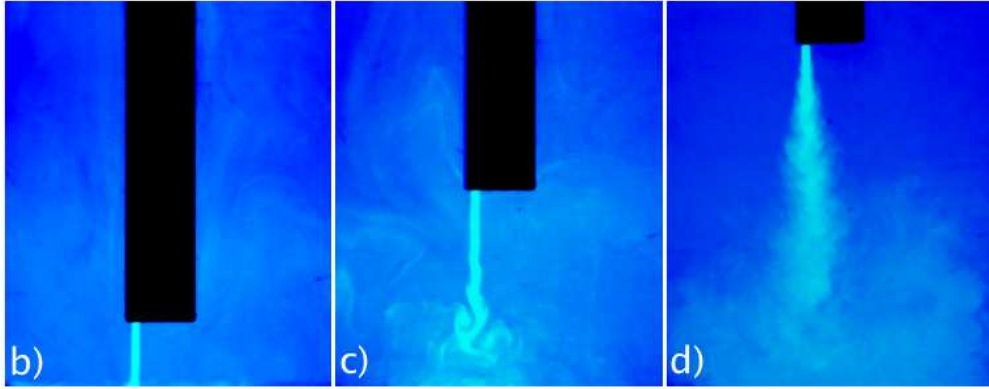
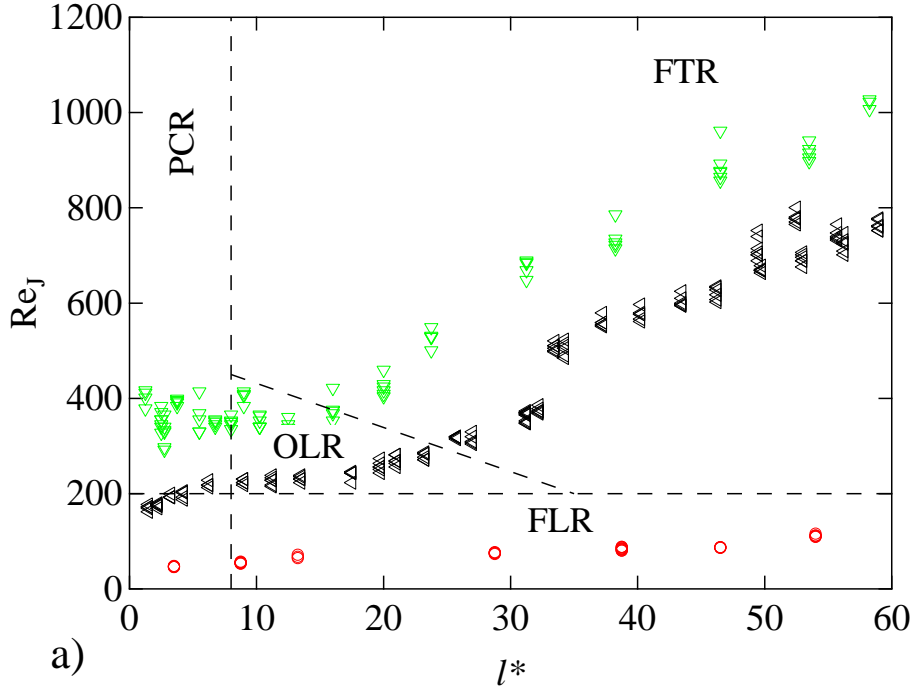


FIG. 2. (a) Jet Reynolds number Re_J at the erosion threshold as a function of the non dimensional nozzle-sediment distance l^* for glass beads of diameter (\triangleleft) $d = 0.25\text{mm}$ and (∇) 1 mm in water ($\nu = 10^6\text{ m}^2/\text{s}$), and for (\circ) glass beads of diameter $d = 0.25\text{ mm}$ in a water-glycerol mixing ($\nu = 4 \times 10^6\text{ m}^2\text{s}^{-1}$). (b-c-d) Dye visualizations of the jet in (b) “free laminar” regime (FLR) for $Re_J = 174$ and $l^* = 7.5$, (c) ‘oscillating locked” regime (OLR) for $Re_J = 230$ and $l^* = 25$, and (d) “free turbulent” regime (FTR) for $Re_J = 804$ and $l^* = 43$.

periodic self-sustained oscillations in the range $200 \lesssim Re_J \lesssim 400$.³⁷ The jet is not free anymore but locked with the back flow induced by the bottom endwall. This regime has been observed³⁷ to exist in a zone of triangular shape reported in Fig. 2a and our own dye jet visualizations confirm the existence of such jet oscillations in this zone (Fig. 2c). Four jet

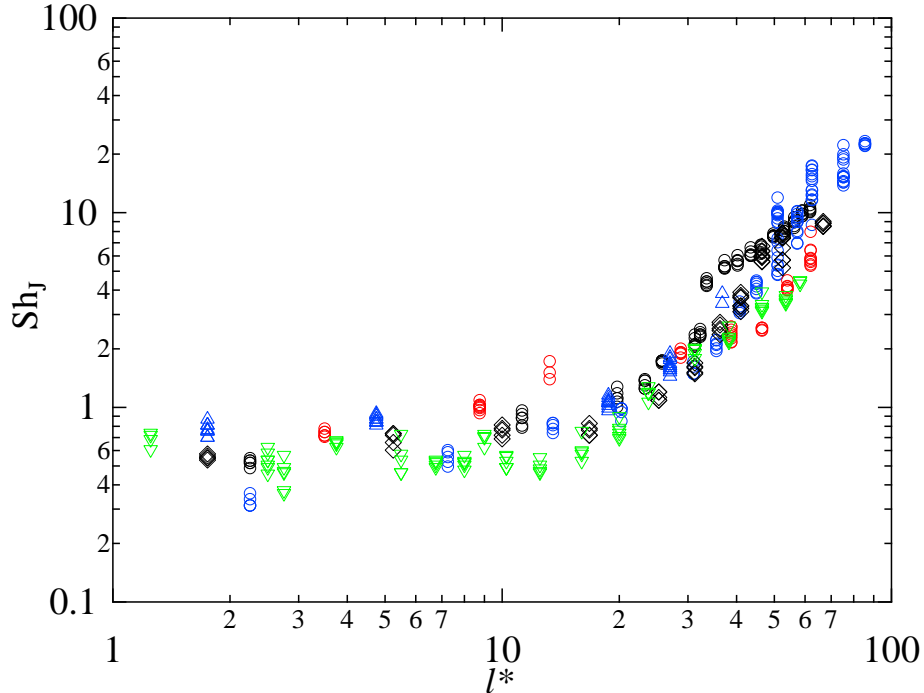


FIG. 3. Jet Shields number Sh_J at the erosion threshold as a function of the non dimensional nozzle-sediment distance l^* for glass beads of different diameters d and fluids of different viscosities ν : (\square) $d = 0.1$ mm, (\triangleleft) $d = 0.25$ mm, (\diamond) $d = 0.35$ mm, (\triangle) $d = 0.5$ mm and (∇) $d = 1$ mm in water ($\nu = 10^6$ m²s⁻¹) and $d = 0.25$ mm in water-glycerol mixing (\triangleright) $\nu = 1.6 \cdot 10^6$ m²s⁻¹ and (\circ) $\nu = 4 \times 10^6$ m²s⁻¹.

“regimes” thus appear in the (Re_J, l^*) diagram of Fig. 2: (i) the “free laminar” regime (FLR) for $Re_J \lesssim 200$, (ii) the “oscillating locked” regime (OLR) in a triangular zone corresponding to $8 \lesssim l^* \lesssim 35$ and $200 \lesssim Re_J \lesssim 400$, (iii) the “free turbulent” regime (FTR) for larger Re_J and l^* values, and (iv) the “potential core” regime (PCR) at small enough l^* . Note that the vertical dashed line $l^* = 8$ has been plotted in Fig. 2 as the upper boundary of PCR although this value may depend slightly on the Reynolds number Re_J with an asymptotic value 5 ± 1 classically reported at large Re_J . A detailed inspection of the data reported in Fig. 2a reveals that if all the data for the grains of diameter $d = 0.25$ mm immersed in a fluid of four times the water viscosity belong to FLR, the two other data sets cross three regimes with increasing jet-bed distance l^* from FLR or PCR to FTR via OLR.

Before analyzing in details the jet regime consequence on the data, let us first look at the corresponding critical Shields number for erosion threshold in Fig. 3 plotted as a function of

the non dimensional jet-bed distance l^* . The three data sets of Fig. 2a, but also other data sets corresponding to other grain diameters and other fluid viscosities, appear to gather in a kind of master curve where the inertial Shields Sh_J would be the pertinent control parameter for erosion in the present case as already observed by other authors in similar configurations.^{8,25,26} A quick inspection of Fig. 3 seems to reveal two behaviors: A constant or quasi constant Shields number at moderate nozzle-sediment distances ($l^* \lesssim 20$), followed beyond by a sharp increase of power law $Sh_J \sim l^{*\alpha}$ for $l^* \gtrsim 20$ with a power exponent α which seems larger than one. We will show in the following that the $Sh_J(l^*)$ relation is not so simple and must be studied in details by a careful analysis of the jet regimes.

IV. DISCUSSION

Laminar or turbulent plane jets from rectangular pipes of large aspect ratio ($w_J/b \gg 1$) can be described by 2D auto-similar models. The evolution of the jet velocity field with the non dimensional distance $x^* = x/b$ from the jet nozzle are usually split into different domains defined by the decay rate of the axial velocity u_0 downstream (or its mean value in turbulent regime). Just outside the nozzle, the jet consists of two shear layers separated by a potential core in which u_0 remains constant along distances x from the jet origin up to $x^* \simeq 5$ at least. For $x^* \gtrsim 5$, the decreasing downstream evolution of $u_0(x)$ can be seen as governed by 2D auto-similar solutions with a virtual jet origin that may not coincide with the outlet but is located at a distance λ from the outlet so that the effective distance to be considered should be $x + \lambda$ instead of x .^{38,39}

For the “free laminar” jet regime at low enough jet Reynolds number ($Re_J \lesssim 200$), we consider that the axial velocity $u_0(x)$ of the jet is given by the classical 2D auto-similar model of a free laminar infinite plane jet:³⁸

$$\frac{u_0(x^*)}{U_J} = \frac{3}{10} \left(\frac{5 Re_J}{x^* + \lambda^*} \right)^{1/3}, \quad (1)$$

where the virtual origin depends on the jet Reynolds number according to the law $\lambda^* = \lambda/b = 0.026 Re_J$.⁴⁰ Note that $\lambda > 0$ so that the virtual origin is here located upstream of the nozzle. By considering that the local velocity u_l at the bed surface is the one given by this free jet model at $x^* = l^*$ and must be the same at erosion threshold for the same fluid/grains configuration whatever the distance l^* , Eq. (1) implies that U_J must scale as $(l^* + \lambda^*)^{1/4}$

at threshold. Figure 4a shows in a logarithmic plot the evolution of the jet velocity U_J at erosion threshold as a function of $l^* + \lambda^*$ for a granular bed made of 0.25 mm glass beads immersed in a water-glycerol mixture of kinematic viscosity $\nu = 4 \times 10^{-6} \text{ m}^2/\text{s}$ that appears to belong to the “free laminar” regime in the (Re_J, l^*) diagram of Fig. 2a. Experimental points line up well along a straight line of slope 1/4 which shows that the present erosion criterion of constant local velocity at the bed surface seems to be appropriate. The found value $u_l = 5.4 \pm 0.4 \text{ cm/s}$ corresponds to the local Shields number $Sh_l = \rho u_l^2 / (\rho_s - \rho)gd \simeq 1$. Note that this extracted velocity for erosion arises from a free jet model with no confinement whereas in the present configuration the jet impinges the bed surface and thus the velocity of the jet must decrease strongly near the bed to vanish at its surface at $x^* = l^*$. As this strong decrease occurs in a very short region, the present result shows that the critical velocity for erosion is given by the “free jet” velocity that would exist at the bed surface. Note also that some data points deviate from the straight line in Fig. 4a for the highest U_J and l^* . This deviation may come both from a jet Reynolds number that approaches the critical transition value to turbulence and from the influence of the experimental finite jet aspect ratio ($w_J/b = 6$) together with the presence of two confining sidewalls ($W/b = 7.5$). The present modeling of FLR data by model Eq. (1) leads to the scaling $Sh_J \sim (l^* + \lambda^*)^{1/2}$. Thus the corresponding data points in the plot $Sh_J(l^*)$ of Fig. 3 should not present any simple scaling in the range $3 \lesssim l^* \lesssim 50$ neither the previously evoked non monotonic dependence with a plateau followed by a rapid increase, as reveal a careful inspection of Fig. 3

For a turbulent sheet jet flow issuing from rectangular nozzle of finite aspect ratio w_J/b , the decay rate of the mean velocity downstream the potential core is highly influenced by the aspect ratio and also by the presence of confining solid sidewalls and even top end walls.^{21,22} For our present configuration of rectangular jet of aspect ratio $w_J/b = 6$ and Reynolds range ($Re_J \sim o(10^3)$), we consider that the axial velocity $u_0(x)$ of our “free” turbulent jet downstream the potential core is given by the decay law:²⁰

$$\frac{u_0(x^*)}{U_J} = \frac{K}{(x^* + \lambda^*)^{1/2}}, \quad (2)$$

where $K \simeq 2$ and $\lambda^* < 0$ so that the virtual origin is here located downstream the jet nozzle close to the end of the potential core. By considering again that the local velocity u_l at the bed surface is the one given by this free jet model at $x^* = l^*$ and must be the same at erosion threshold for the same fluid/grains configuration whatever the distance l^* , Eq. (2) implies

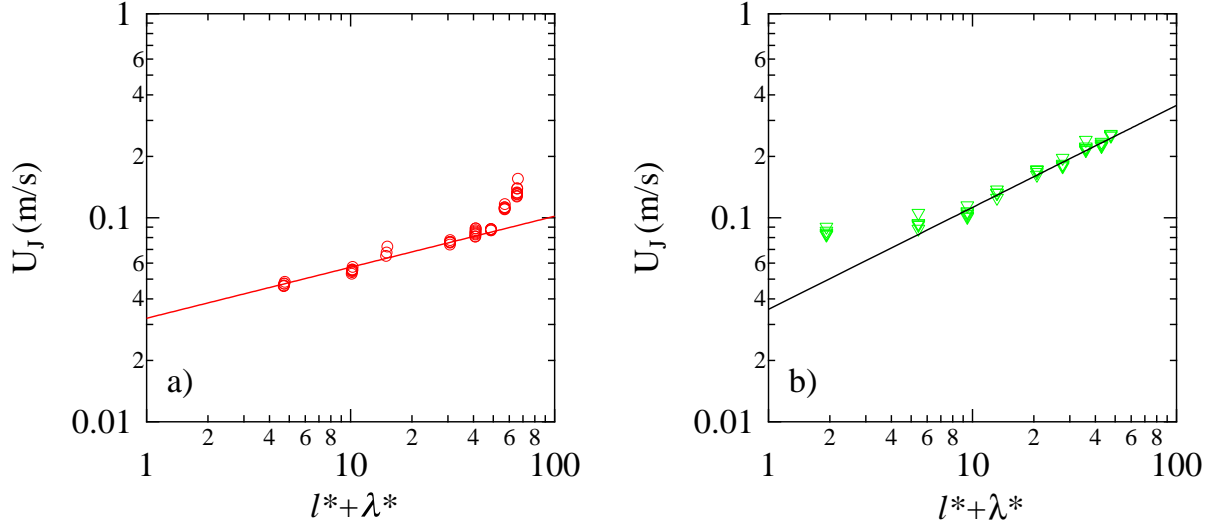


FIG. 4. Jet velocity U_J at erosion threshold as a function of the non dimensional distance $l^* + \lambda^*$ of the bed surface from the jet virtual origin for (a) glass beads of diameter $d = 0.25$ mm immersed in a water-glycerol mixture ($\nu = 410^6 \text{m}^2/\text{s}$) and (b) glass beads of diameter $d = 1$ mm immersed in water ($\nu = 10^6 \text{m}^2/\text{s}$). (—) Fit from self-similar (a) laminar (Eq. 1) or (b) turbulent (Eq. 2) models.

that U_J must scale as $(l^* + \lambda^*)^{1/2}$ at threshold. Figure 4b shows the evolution in a logarithmic plot of the jet velocity U_J at erosion threshold as a function of the normalized distance $l^* + \lambda^*$ from the jet virtual origin of a granular bed made of 1 mm glass beads immersed in water. Experimental points line up along a straight line of slope 1/2, except data points at too small l^* ($l^* \lesssim 15$) corresponding to a jet in the “oscillating locked” regime or “potential core regime”. This shows that the local velocity u_l at erosion threshold predicted by this model is constant with the fitting value $u_l = 8 \pm 0.5$ cm/s, corresponding to the local Shields number $Sh_l \simeq 0.4$. Note that this fitting value u_l is very close to the plateau value $U_J = 8 \pm 1$ cm/s that can be observed to appear at low $l^* + \lambda^*$ values corresponding to the potential core. This is very satisfying and validates the present modeling. It appears in particular that our experimental plane jet does not seem to turn into a 3D axisymmetric circular jet as reported by Krothapalli *et al.*¹⁹ for high distances x^* since our data correspond here to low enough l^* ($l^* \lesssim 60$). Note also that the extracted critical velocity for erosion arises from a free jet model with no bottom endwall whereas in the present configuration the jet impinges the bed surface so that the velocity of the jet decreases strongly near the bed to vanish at its

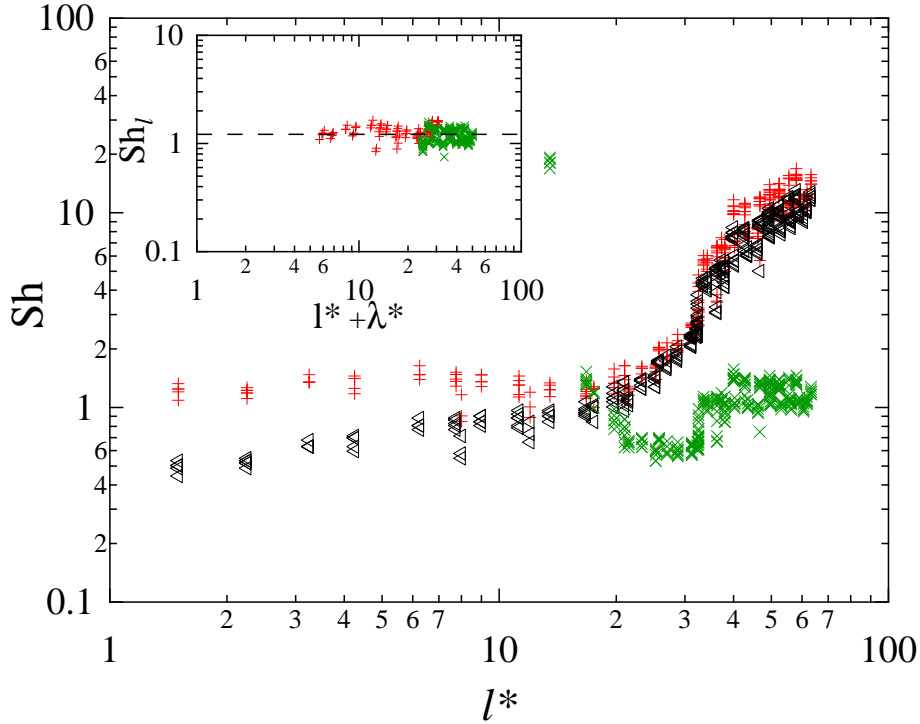


FIG. 5. Shields number as a function of the non dimensional jet-bed distance l^* for glass beads of diameter $d = 0.25\text{mm}$ in water. (\triangleleft) Global values Sh_J and ($+$, \times) local values Sh_l calculated ($+$) from laminar model eq. (1) and (\times) turbulent model eq. (2). In the inset local Shields number as a function of the non dimensional distance $l^* + \lambda^*$ of the bed from the jet virtual origin.

surface at $x^* = l^*$. As this strong decrease occurs in a very short region of order $l/10$ above the bottom end wall, the present result shows that the critical velocity for erosion is given by the “free jet” velocity that would exist at the bed surface. Note that in the $U_J(l^* + \lambda^*)$ logarithmic plot of Fig. 4b, the value $\lambda^* \simeq -10$ was found from a $aU_J^2(l^*)$ linear plot in which λ^* corresponds to the y -intercept of a linear fit through the data. The correct modeling of FTR data by model Eq. (2) leads thus to the scaling $Sh_J \sim (l^* + \lambda^*)$ which explains why Sh_J does not evolve linearly with l^* in Fig. 3 for high l^* . For $l^* \lesssim 10$, U_J remains constant as the jet is in the potential core regime (PCR) so that Sh_J remains constant which explains the plateau observed in Fig. 3 at low l^* .

Let us now look how this complex $Sh_J(l^*)$ curve of Fig. 3 is transformed in a $Sh_l(l^*)$ plot for the last data set presented in Fig. 2a and that passes from FLR to FTR via OLR. This is shown in Fig. 5 where the set of Sh_J values are displayed together with the two sets of

Sh_l values calculated either from the laminar model (Eq. 1) and turbulent model (Eq. 2). We see that the Sh_l values calculated from the laminar model align onto a plateau when corresponding to FLR (and also OLR), whereas those corresponding to FTR deviate from that plateau increasingly with l^* . This shows that the laminar model is correct in the whole laminar regime and strongly fails in the turbulent regime as expected. Note that the plateau value of Sh_l appears surprisingly larger than the corresponding Sh_j values. This is due to the fact that Sh_j is defined with the mean jet velocity U_j whereas Sh_l is calculated with the axial velocity that may be up to $(3/2)U_j$ at the nozzle exit for a well established laminar Poiseuille profile so that Sh_l may be up to $(9/4)Sh_j$. Inversely, the Sh_l values calculated from the turbulent model align also onto a plateau when corresponding to FTR showing that the turbulent model is correct for FTR only and fails in the other regimes as expected. In the transition zone between laminar and turbulent regimes, here for $20 \lesssim l^* \lesssim 30$, both models fail. However, when Sh_l is plot against $l^* + \lambda^*$ in the inset of Fig 5, there is no gap anymore but a small overlap between the two sets of data points belonging to each plateau. This is due to the change in the sign of λ from positive values in the laminar regime to negative values in the turbulent regime. It is worthnoting that the Sh_l plateau value arising from turbulent data is the same as the Sh_l plateau value arising from laminar data, with the value $Sh_l \simeq 1$. It thus seems that the nature (turbulent or laminar) of the jet does not have a significant influence on the erosion threshold.

The local Shields number Sh_l at erosion threshold in laminar or turbulent regimes have been determined for all the data sets of Fig. 3 by either the laminar or turbulent free jet model (Eqs (1) or (2)). Figure 6 displays the averaged values from both models as a function of the *local particle* Reynolds number $Re_p = u_l d / \nu$ based on the local velocity u_l and the grain diameter d . All values appear around $Sh_l \simeq 1$ for a particle Reynolds number always larger than one: $3 \lesssim Re_p \lesssim 10^2$. The fact that the relevant parameter characterizing erosion is here an *inertial* Shields number is thus related to large enough Re_p values ($Re_p > 1$). The critical Sh_l values for erosion that would be given by a viscous local Shields number based on the local viscous force $\eta u_l d$ instead of the inertial one $\rho u_l^2 d^2$ would be smaller and would decrease as $1/Re_p$: a viscous Shields number would thus not be relevant in the present study, contrary to parallel shearing flow configurations.^{30,41}

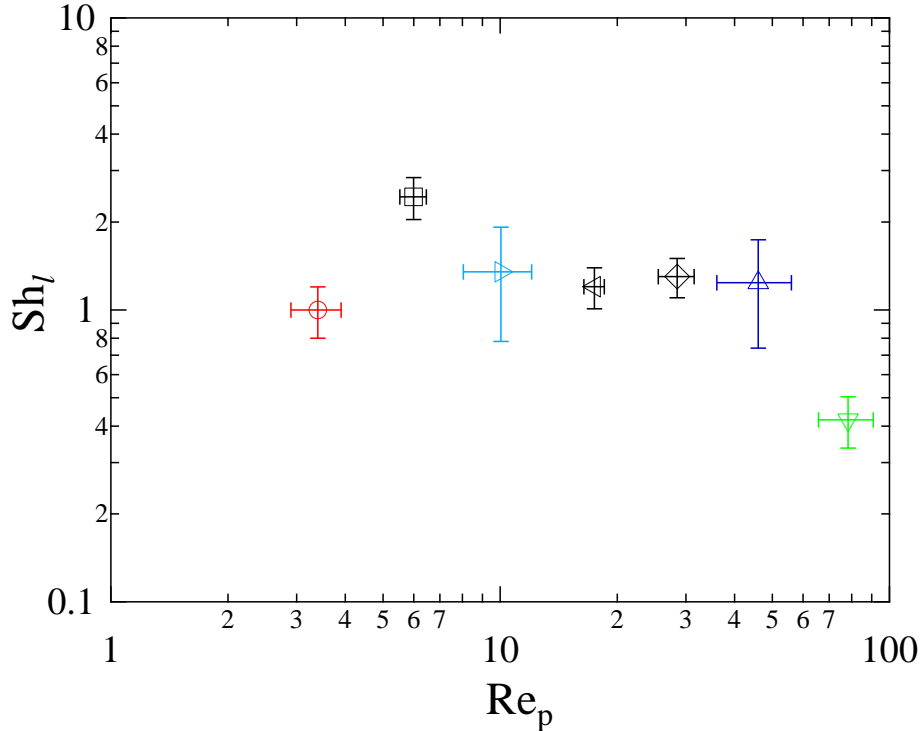


FIG. 6. Local Shields number Sh_l as a function of the particle Reynolds number Re_p . Same symbols as in Fig.3.

V. CONCLUSION

We have studied experimentally the erosion threshold of a liquid immersed granular bed made of glass beads by an impinging plane liquid jet, either laminar or turbulent, as a function of the nozzle-sediment distance l in a model quasi 2D set-up. We have shown that the erosion threshold is well characterized by a critical Shields number Sh_l of inertial nature, which increases non-uniformly with l . This non-uniform evolution has been shown to be linked to the spatial evolution of the jet related to its flow regime. Using auto-similar models in either laminar or turbulent jet regimes, the local jet erosion velocity at the bed surface has been extrapolated and shows that the corresponding local inertial Shields number Sh_l characterizes well the erosion threshold, with the critical value $Sh_{lc} \simeq 1$ in the corresponding range of local particle Reynolds number larger than one. In the turbulent regime this leads to the following dependance of the critical global Shields number for erosion: $Sh_{Jc} \simeq 1$ for $l^* \lesssim |\lambda^*|$ and $Sh_{Jc} \simeq (l^* + \lambda^*)/K^2$ for $l^* \gtrsim |\lambda^*|$, which for the present nozzle

aspect ratio $w_J/b = 6$ reads $Sh_{Jc} \simeq 0.25(l^* - 10)$ for $l^* \gtrsim 10$. This linear law is the same as the usual one²⁶ corrected by the effect of the jet virtual origin λ^* . In the laminar regime the erosion threshold in terms of the global Shields number is governed for all l^* by the non linear law $Sh_{Jc} \simeq 11(l^*/5Re_J)^{2/3}$ even though the correction for the virtual origin is negligible. This detailed study of the erosion threshold with the jet structure may be useful for a better understanding of the subsequent cratering beyond threshold where the shape modification of the surface affects the impingement flow structure, and could help for the validation of new numerical methods.^{42,43}

The authors thank L. Auffray, P. Jenffer, G. Marteau and R. Pidoux for their help in the design and realization of the experimental setup and J. Giez and A. Soulier for preliminary experiments. This work benefits from fruitful discussions with D. Salin, D. Doppler, D. Pham-Van-Bang, C. Chevalier, P. Pinnettes, P. Philippe, S. Bonelli and J.Y. Delenne, and from the financial support of the ANR (STABINGRAM project NO. 2010-BLAN-0927-01).

REFERENCES

- ¹B. Andreotti, Y. Forterre, and O. Pouliquen, *Granular Media: Between Fluid and Solid* (Cambridge University Press, 2013).
- ²F. Graveleau, J.-E. Hurtrez, S. Dominguez, and J. Malavieille, “A new experimental material for modeling relief dynamics and interactions between tectonics and surface processes,” *Tectonophysics*, **513**, 68 – 87 (2011), ISSN 0040-1951.
- ³B. A. Hamm, W. L. West, and G. B. Tatterson, “Sludge suspension in waste storage tanks,” *AICHE Journal*, **35**, 1391–1394 (1989), ISSN 1547-5905.
- ⁴T. E. Lee, J. G. Leishman, and M. Ramasamy, “Fluid dynamics of interacting blade tip vortices with a ground plane,” *Journal of the American Helicopter Society*, **55**, 22005–1–16 (2010).
- ⁵P. Metzger, C. Immer, C. Donahue, B. Vu, R. Latta, and M. Deyo-Svendsen, “Jet-induced cratering of a granular surface with application to lunar spaceports.” *J. Aerospace Eng.*, **2** (2009).
- ⁶M. Foster, R. Fell, and M. Spannagle, “The statistics of embankment dam failures and accidents,” *Canadian Geotechnical Journal*, **37**, 1000–1024 (2000).

- ⁷C. Wan and R. Fell, “Laboratory tests on the rate of piping erosion of soils in embankment dams,” *Geotechnical Testing Journal*, **27** (2004).
- ⁸G. Hanson and K. Cook, “Apparatus, test procedures, and analytical methods to measure soil erodibility in situ,” *Applied Engineering in Agriculture*, **20**, 455–462 (2004).
- ⁹P.-H. Yeh, K.-A. Chang, J. Henriksen, B. Edge, P. Chang, A. Silver, and A. Vargas, “Large-scale laboratory experiment on erosion of sand beds by moving circular vertical jets,” *Ocean Engineering*, **36**, 248 – 255 (2009).
- ¹⁰T. N. Hunter, J. Peakall, T. J. Unsworth, M. H. Acun, G. Keevil, H. Rice, and S. Biggs, “The influence of system scale on impinging jet sediment erosion: Observed using novel and standard measurement techniques,” *Chemical Engineering Research and Design*, **91**, 722 – 734 (2013), ISSN 0263-8762.
- ¹¹K. Jambunathan, E. Lai, M. Moss, and B. Button, “A review of heat transfer data for single circular jet impingement,” *International Journal of Heat and Fluid Flow*, **13**, 106 – 115 (1992).
- ¹²M. Desphande and R. Vaishnav, “Submerged laminar jet impingement on a plane,” *J. Fluid Mech.*, **114**, 213–236 (1982).
- ¹³C. Ho and P. Huerre, “Perturbated free shear layers,” *Annual Review of Fluid Mechanics*, **16**, 365–424 (1984).
- ¹⁴D. Phares, G. Smedley, and R. Flagan, “The wall shear stress produced by the normal impingement of a jet on a flat surface,” *J. Fluid Mech.*, **418**, 351–375 (2000).
- ¹⁵M. Kristiawan, A. Meslem, I. Nastase, and V. Sobolik, “Wall shear rates and mass transfer in impinging jets: Comparison of circular convergent and cross-shaped orifice nozzles,” *International Journal of Heat and Mass Transfer*, **55**, 282 – 293 (2012), ISSN 0017-9310.
- ¹⁶S. Beltaos and N. Rajaratnam, “Plane turbulent impinging jets,” *Journ. of Hydr. Res.*, **11**, 29–59 (1973).
- ¹⁷G. Gutmark and I. Wygnanski, “The planar turbulent jet,” *J. Fluid Mech.*, **73**, 465–495 (1976).
- ¹⁸S. Maurel and C. Sollicec, “A turbulent plane jet impinging nearby and far from a flat plate,” *Experiments in Fluids*, **31**, 687–696 (2001).
- ¹⁹A. Krothapalli, D. Baganoff, and K. Karamcheti, “On the mixing of rectangular jets.” *J. Fluid Mech.*, **107**, 201–220 (1981).
- ²⁰L. P. Chua and A. C. Lua, “Measurements of a confined jet,” *Physics of Fluids*, **10**, 3137–

- 3144 (1998).
- ²¹R. Deo, J. Mi, and G. Nathan, “The influence of nozzle aspect ratio on plane jets,” *Experimental Thermal and Fluid Science*, **31**, 825 – 838 (2007), ISSN 0894-1777.
- ²²M. Alnahhal, A. Cavo, A. Romeos, K. Perrakis, and T. Panidis, “Experimental investigation of the effect of endplates and sidewalls on the near field development of a smooth contraction rectangular jet,” *European Journal of Mechanics - B/Fluids*, **30**, 451 – 465 (2011), ISSN 0997-7546.
- ²³R. cant, I. Castro, and P. Walklate, “Plane jets impinging on porous wall,” *Experiments in Fluids*, **32**, 16–26 (2002).
- ²⁴S. Webb and I. Castro, “Axisymmetric jets impinging on porous walls,” *Experiments in Fluids*, **40**, 951–961 (2006), ISSN 0723-4864, 10.1007/s00348-006-0131-z.
- ²⁵N. Rajaratman and S. Beltaos, “Erosion by impinging circular jets.” *Procs. ASCE, J. Hydr. Div.*, **103**, 1191–1205 (1977).
- ²⁶N. Rajaratnam, “Erosion by plane turbulent jets,” *Journal of Hydraulic Research*, **19**, 339–358 (1981).
- ²⁷O. Aderibigbe and N. Rajaratnam, “Erosion of loose beds by submerged circular impinging vertical turbulent jets,” *Journal of Hydraulic Research*, **34**, 19–33 (1996).
- ²⁸S. Kuang, C. LaMarche, J. Curtis, and A. Yu, “Discrete particle simulation of jet-induced cratering of a granular bed,” *Powder Technology*, **239**, 319 – 336 (2013), ISSN 0032-5910.
- ²⁹H. M. Charru, F. and O. Eiff, “Erosion and deposition of particles on a bed sheared by a viscous flow,” *J. Fluid Mech*, **519**, 55–80 (2004).
- ³⁰T. Loiseleux, P. Gondret, M. Rabaud, and D. Doppler, “Onset of erosion and avalanche for an inclined granular bed sheared by a continuous laminar flow,” *Physics of Fluids*, **17**, 103304 (2005).
- ³¹V. Vanoni, “Sediment transportation mechanics: initiation of motion,” *J. Hydr. Div*, **92**, 291 (1966).
- ³²C. Dancey, P. Diplas, A. Papanicolaou, and M. Bala, “Probability of individual grain movement and threshold condition,” *Journal of Hydraulic Engineering*, *Journal of Hydraulic Engineering*, **128**, 1069–1075 (2002).
- ³³A. Wierschem, C. Groh, I. Rehberg, N. Aksel, and C. A. Kruehle, “Ripple formation in weakly turbulent flow,” *Eur. Phys. J. E*, **25**, 213–221 (2008).
- ³⁴G. Gioia and F. A. Bombardelli, “Localized turbulent flows on scouring granular beds,”

- Phys. Rev. Lett., **95**, 014501 (2005).
- ³⁵F. A. Bombardelli and G. Gioia, “Scouring of granular beds by jet-driven axisymmetric turbulent cauldrons,” *Physics of Fluids*, **18**, 088101 (2006).
- ³⁶R. J. Munro, N. Bethke, and S. B. Dalziel, “Sediment resuspension and erosion by vortex rings,” *Physics of Fluids*, **21**, 046601 (2009).
- ³⁷A. Maurel, P. Ern, B. J. A. Zielinska, and J. E. Wesfreid, “Experimental study of self-sustained oscillations in a confined jet,” *Phys. Rev. E*, **54**, 3643–3651 (1996).
- ³⁸D. Tritton, *Physical Fluid Dynamics*, 2nd ed. (Oxford, 1988).
- ³⁹N. E. Kotsovinos, “A note on the spreading rate and virtual origin of a plane turbulent jet,” *Journal of Fluid Mechanics*, **77**, 305–311 (1976), ISSN 1469-7645.
- ⁴⁰A. Revuelta, A. L. Sánchez, and A. Linánnán, “The virtual origin as a first-order correction for the far-field description of laminar jets,” *Physics of Fluids*, **14**, 1821–1824 (2002).
- ⁴¹M. Ouriemi, P. Aussillous, M. Medale, Y. Peysson, and E. Guazzelli, “Determination of the critical shields number for particle erosion in laminar flow,” *Physics of Fluids*, **19**, 061706 (2007).
- ⁴²K. N. D. Pham Van Bang and M. U. Zapata, “Two-phase study of erosion by a vertical jet,” in *Proc. of the 2nd Two-pHase modElling for Sediment dynamIcS* (2013).
- ⁴³F. Mercier, S. Bonelli, F. Anselmet, P. Pinettes, J. Courivaud, and J. Fry, “On the numerical modelling of the jet erosion test,” in *ICSE6, August 27-31, 2012, Paris* (2012).